



Comparative studies on formation and material characterization of L-histidine derivatives for nonlinear optical device applications

Helen Merina Albert^{1,*}  and C. Alosious Gonsago²

¹Department of Physics, Sathyabama Institute of Science and Technology, Chennai 600119, India

²Department of Electronics Science, Mohamed Sathak College of Arts and Science, Chennai 600119, India

Received: 19 October 2021

Accepted: 29 November 2021

Published online:

9 January 2022

© The Author(s), under exclusive licence to Springer Science+Business Media, LLC, part of Springer Nature 2021

ABSTRACT

In this study, nonlinear optical crystalline materials L-histidinium hydrochloride monohydrate (LHHCL) and L-histidinium methyl ester dihydrochloride (LHMDHCL) were successfully grown by slow solvent evaporation technique. As-grown crystalline materials were subjected to X-ray structure analysis, FT-Raman spectroscopy, energy-dispersive X-ray spectroscopy, UV–Vis spectroscopy, frequency conversion analysis, dielectric and Vicker's microhardness studies. According to XRD data, the grown crystal LHHCL was crystallized to an orthorhombic form having a space group $P2_12_12_1$, while LHMDHCL crystal belongs to a monoclinic form with a space group $P2_1$. The FT-Raman study confirms the existence of chemical groups and the formation of two different crystals. The chemical compositions of the as-grown crystalline materials were established by Energy-dispersive X-ray spectroscopy. The UV–Vis study substantiates the transparency of LHHCL and LHMDHCL in the wavelength regions of 232–1000 nm and 230–1000 nm, respectively. Using the Tauc equation, the bandgap energy was determined as 5.35 eV and 5.38 eV for LHHCL and LHMDHCL crystals, respectively. In addition, the grown crystals have shown a better frequency conversion efficiency in comparison to KDP samples. According to the dielectric study, dielectric characteristics such as dielectric constant and dielectric loss for the LHHCL and LHMDHCL crystals drop as frequency increases. The hardness of the LHHCL and LHMDHCL crystals was measured by Vickers microhardness test which reveals that the grown crystals follow the normal indentation size effect.

Address correspondence to E-mail: drhelenphy@gmail.com

1 Introduction

The growth of new crystalline materials for the frequency conversion process in the ultra-violet to the near infra-red spectral region continues to be a significant demand. High-quality crystalline materials having enhanced performance will still be in demand for nonlinear optical device applications. Due to their potential applications in laser technology, optical communication, optical switching, optical mixing, optical power limiting data storage, image processing, and electro-optic applications, nonlinear optical materials have sparked considerable attention in recent years [1–9]. Generally, molecules in organic compounds are linked by weaker Vander Waals interactions or h-bonding, and it leads to poor thermal or mechanical strength. Semi-organic mixed materials are investigated for optical applications in an attempt to address these difficulties. Amino acid-inorganic salt complexes have attracted researcher interest as they have physicochemical properties, including optical transparency, high laser damage threshold, and second harmonic generation [10, 11]. In semi-organic compounds, the organic molecules are also stoichiometrically bonded to appropriate inorganic counterparts or metal ions, which improve the specimen's hardness and thermal strength [12–14]. Furthermore, in the solid form, amino acids are frequently dipolar, having an electron donor and acceptor group on each molecule. As a result of their dipolar characteristics, amino acids are being considered as potential nonlinear possibilities. [15, 16].

L-histidine, an amino derivative, has been actively explored since the development of L-histidine tetrafluoroborate, a potential NLO material. According to Marcy et al., the magnitude of nonlinear optical efficiency of L-histidine tetrafluoroborate would be five times better than those of typical KDP samples [17]. As a result, L-histidine analogs such as L-histidine acetate, L-histidine hydrofluoride, L-histidine perchloride, L-histidine nitrates, L-histidine sulfates, L-histidine bromide, L-histidine maleates, L-histidine dihydrogen tetrafluoroborate, L-histidine trifluoroacetate, L-histidinium glutarate monohydrate, L-histidine cadmium chloride, and L-histidinium iodide have been developed [18–29].

In continuance of prior works, we synthesized orthorhombic form of L-histidinium hydrochloride monohydrate (LHHCL) and monoclinic form of L-

histidinium methyl ester dihydrochloride (LHMDHCL) using the slow solvent evaporation method with water as a solvent. Donohue and Caron were the first to publish the original structure of L-histidinium hydrochloride monohydrate, whereas Vilchiz et al., were the first to define the actual structure of L-histidine methyl ester dihydrochloride [30, 31]. In this investigation, XRD, FT-Raman, EDAX, UV-Vis spectroscopic analyses, as well as SHG, dielectric, and hardness tests were used to characterize the as-grown LHHCL and LHMDHCL crystals.

2 Materials and methods

Analytical grade L-histidine, hydrochloric acid, and L-histidinium methyl ester dihydrochloride, procured from Merck India, were used to form LHHCL and LHMDHCL crystals. The L-histidinium hydrochloride monohydrate (LHHCL) was formed by dissolving a stoichiometric ratio of L-histidine and hydrochloric acid into the double-distilled water. The prepared solution was continuously stirred for about 6 h using a magnetic stirrer until a homogeneous mixture over the entire volume was formed. Tiny colorless crystalline samples were obtained by heating the obtained mixture to dryness below an optimum temperature (55 °C) in a temperature-controlled water bath. Again, these crystalline samples were thoroughly dissolved in double distilled water to get a well-saturated solution [32, 33]. The other material L-histidinium methyl ester dihydrochloride was re-extracted using distilled water for the formation of LHMDHCL crystal. The purified LHMDHCL was entirely dissolved into the double distilled water at room temperature and properly homogenized using a magnetic stirrer. Then, to remove undesirable contaminants, both the LHHCL and LHMDHCL mixtures were then filtered thrice with micro-filter sheets. These solutions were stored in two separate beakers with porous paper coverings to allow for slow solvent evaporation. The beakers were put in a water bath at 32 °C for ensuring a steady growth rate. In this experiment, 2 drops of H₂O₂ were applied to the LHHCL and LHMDHCL mixtures to suppress the growth of any microbes. After a month, the LHHCL and LHMDHCL crystals of optimal size were formed, as illustrated in Fig. 1.

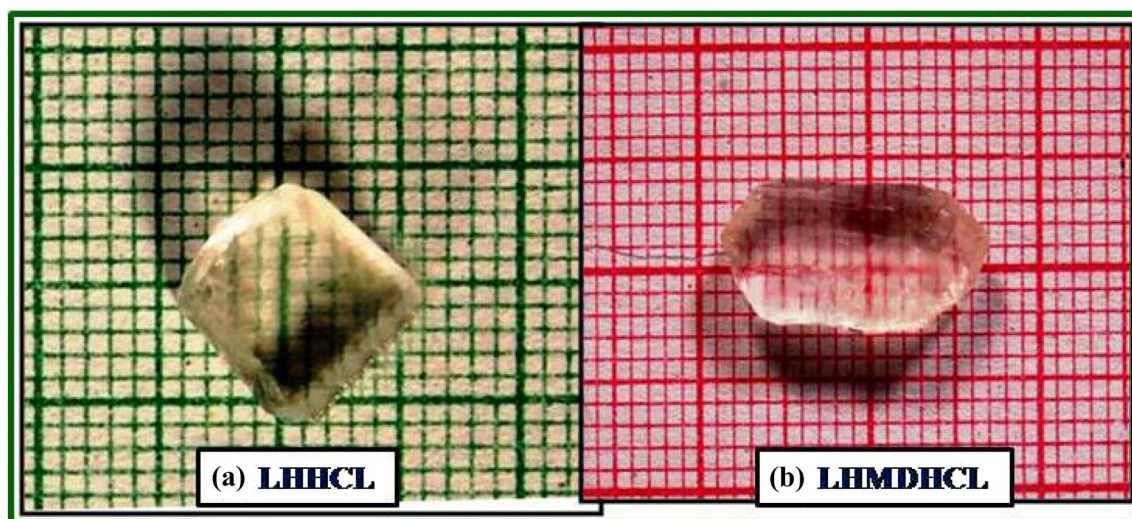


Fig. 1 Pictures of **a** LHHCL and **b** LHMDHCL

3 Results and discussion

3.1 X-ray diffraction study

Typical X-ray diffraction study is a non-destructive technique for evaluating the three-dimensional structure of crystalline substances and measuring molecular dimensions with precision and accuracy. A Bruker-axs-kappa-apex2-CCD diffractometer with M_oK_α ($\lambda = 0.71073 \text{ \AA}$) radiation source has been used for diffraction analysis. Tiny samples with dimensions of $0.10 \times 0.15 \times 0.35 \text{ mm}^3$ were sliced from the test crystals and used for further measurements. According to crystallographic data, the LHHCL crystal has an orthorhombic form and a $P2_12_12_1$ space group, whereas the LHMDHCL crystal has a monoclinic form and a $P2_1$ space group. Also, LHHCL has cell parameters of $a = 15.285 (\pm 0.032) \text{ \AA}$; $b = 8.884 (\pm 0.041) \text{ \AA}$; $c = 6.876 (\pm 0.020) \text{ \AA}$ and $V = 933.71 (\pm 4) \text{ \AA}^3$, while LHMDHCL has cell parameters of $a = 8.221 (\pm 0.023) \text{ \AA}$; $b = 7.108 (\pm 0.015) \text{ \AA}$; $c = 9.505 (\pm 0.052) \text{ \AA}$, $\beta = 94.54^\circ$ and $V = 553.681 (\pm 2) \text{ \AA}^3$. The observed lattice parameters are fairly close to the reported values [30, 31]. Table 1 lists the crystallographic data obtained for LHHCL and LHMDHCL crystals.

3.2 FT-Raman spectral analysis

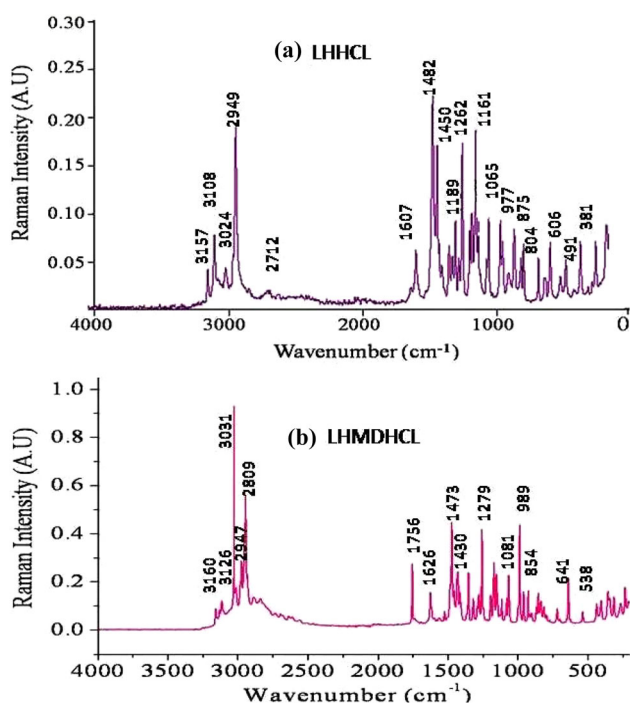
The FT-Raman method is highly beneficial for qualitative analysis and compound detection. The FT-Raman spectral analysis was conducted in the

spectral range $450\text{--}4000 \text{ cm}^{-1}$ with the use of a Bruker- RFS27 FT-Raman instrument. Figure 2 illustrates the recorded Raman spectra of LHHCL and LHMDHCL crystals. The spectral frequencies are elucidated and compared to the well-known spectra [34, 35]. In the case of LHHCL, the peaks recorded around 3157 and 3108 cm^{-1} are expected to be caused by asymmetric and symmetric NH stretch of amine functionality, which is a defining feature of amino acids. Aliphatic and aromatic C–H stretches are responsible for the peaks at 2712 and 3024 cm^{-1} , respectively. The strong peak at 2949 cm^{-1} is caused by $-(CH_2)-$ stretching vibration. Asymmetric and symmetric COO^- stretches are responsible for the peaks at 1553 and 1412 cm^{-1} . Aliphatic and aromatic C–N stretches are responsible for the peaks at 1161 cm^{-1} and 1482 cm^{-1} , respectively. The torsional vibrations of the NH_3^+ group form the peak at 491 cm^{-1} and the C–O stretch is responsible for the peak at 1065 cm^{-1} .

Regarding LHMDHCL crystal, the signals recorded around 3160 and 3126 cm^{-1} are expected to be caused by asymmetric and symmetric NH stretch of amine functionality. Aliphatic and aromatic C–H stretches are responsible for the peaks at 2809 and 3031 cm^{-1} , respectively. The presence of C=O stretch of carbonyl can be seen by the prominent peak at 1756 cm^{-1} . The C=N stretch of the imidazole ring of L-histidine is responsible for the peak at 1626 cm^{-1} . The stretch of the C–O group of ester causes a significant peak at 1279 cm^{-1} . The peaks at 641 , 854 , and 989 cm^{-1} in the relatively low wavenumber region

Table 1 XRD details of LHHCL and LHMDHCL crystals

Crystal	LHHCL	LHMDHCL
Empirical formula	C ₆ H ₁₂ O ₃ N ₃ Cl	C ₇ H ₁₃ O ₂ N ₃ Cl ₂
Formula weight	209.64	242.10
Wavelength	0.71073 Å	0.71073 Å
Crystal system space group	Orthorhombic P2 ₁ 2 ₁ 2 ₁	Monoclinic P2 ₁
Unit cell parameters	$a = 15.285 (\pm 0.032) \text{ \AA}$ $b = 8.884 (\pm 0.041) \text{ \AA}$ $c = 6.876 (\pm 0.020) \text{ \AA}$ $\alpha = \beta = \gamma = 90^\circ$	$a = 8.221 (\pm 0.023) \text{ \AA}$ $b = 7.108 (\pm 0.015) \text{ \AA}$ $c = 9.505 (\pm 0.052) \text{ \AA}$ $\alpha = \gamma = 90^\circ; \beta = 94.56^\circ$
Volume	933.71(± 4) Å ³	553.681(± 2) Å ³
Z	4	2
Calculated density	1.489 Mg m ⁻³	1.451 Mg m ⁻³

**Fig. 2** Raman spectra of **a** LHHCL and **b** LHMDHCL

are caused by plane deformation, ring symmetric, and asymmetric stretch of L-histidine. The prominent peaks of LHHCL and LHMDHCL, which agree with our findings, are listed in Table 2.

3.3 Energy-dispersive X-ray analysis

EDAX is a micro-analytical approach that makes use of X-ray distinctive spectrum generated from the specimen during high-energy excitation of electrons. This technique is useful for determining which elements are present in a particular compound [36, 37]. In this investigation, the EDAX analysis has been

conducted for the given samples using an FEI-QUANTA-200F micro-analyzer. Figure 3 shows the observed spectra of the LHHCL and LHMDHCL samples. Table 3 shows the weight percentages (wt%) of constituent atoms as obtained by EDAX analysis. The presence of oxygen, nitrogen, carbon, and chlorine in the right proportion confirms the formation of the LHHCL and LHMDHCL crystals.

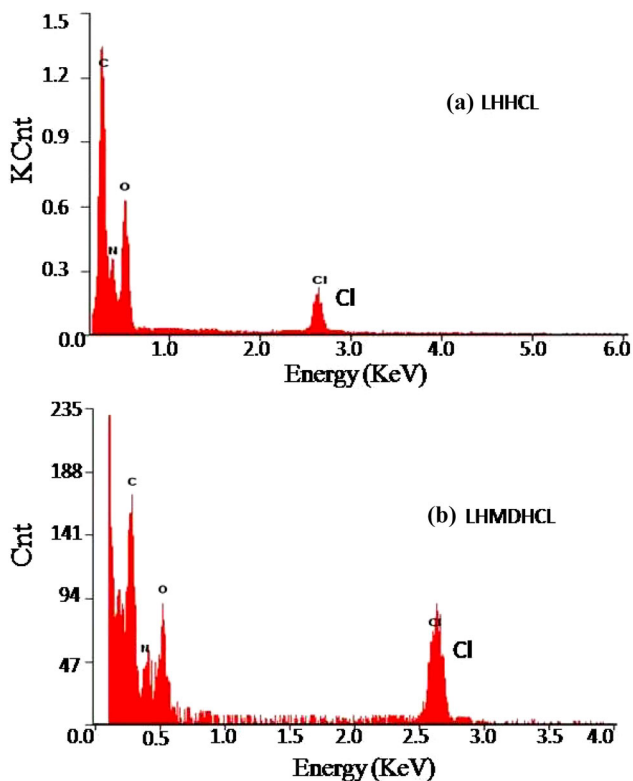
3.4 UV-Vis spectroscopy

The transmittance range and compatibility of the produced crystals for optoelectronic applications were determined using UV-Vis spectroscopic study. The absorbance spectra of the grown crystals were measured spectrophotometrically within the region of 200–1000 nm. The acquired absorbance spectra of LHHCL and LHMDHCL are displayed in Fig. 4. According to the absorption spectra, the LHHCL and LHMDHCL are fully transparent in the UV-Vis range, indicating that they will be suitable materials for nonlinear optical device applications. In addition, the spectra show a significant drop in absorption at 232 nm for LHHCL and 230 nm for LHMDHCL, which correlates to the fundamental absorption wavelengths or absorption edges of the crystals.

The UV-Vis absorption spectra are also helpful in knowing the nature and value of the bandgap energy of the LHHCL and LHMDHCL crystals [38, 39]. The bandgap energy of the LHHCL and LHMDHCL was estimated with the help of UV-Vis spectra by using the Tauc formula [40]. The curves involving $(\alpha h\nu)^2$ and $h\nu$ were drawn and they are given in Fig. 5. The bandgap energy was found by drawing a linear line on the linear portion of the plot at $(\alpha h\nu)^2 = 0$. The bandgap energy of LHHCL is calculated to be 5.35 eV

Table 2 Raman frequency assignments of LHHCL and LHMDHCL crystals

LHHCL (cm ⁻¹)	LHMDHCL (cm ⁻¹)	Assignments
3157	3160	NH asymmetric stretch
3108	3126	NH symmetric stretch
3024	3031	Aromatic C–H stretch
2949	2947	CH ₂ stretch
2712	2809	Aliphatic C–H stretch
–	1756	C=O Stretch of carbonyl group
1607	1626	C=N Stretch of imidazole ring
1553	1567	Asymmetric COO ⁻ stretch
1482	1473	Aromatic C–N stretch
1450	1430	C–C stretch
1412	1414	Symmetric COO ⁻ stretch
–	1279	C–O stretch of ester
1262	1257	CH ₃ stretch
1161	1153	Aliphatic C–N stretch
1065	1081	C–O stretch
977	989	Ring asymmetric stretch
875	854	Ring symmetric stretch
804	836	C–C–O stretch
695	641	Plane deformation
491	538	Torsional oscillation of NH ₃ ⁺

**Fig. 3** EDAX spectra of **a** LHHCL and **b** LHMDHCL

while the bandgap energy of LHMDHCL is calculated to be 5.38 eV. Hence, due to their wide bandgaps, the LHHCL, and LHMDHCL crystals have a

Table 3 EDAX elemental analysis of LHHCL and LHMDHCL

Element	LHHCL Wt%	LHMDHCL Wt%
C	49.78	37.04
N	23.49	27.20
O	19.98	18.40
Cl	06.75	17.36

The bold values signifies the quantitative presence of chlorine atoms in both the LHHCL and LHMDHCL crystals

large transmittance window in the UV–Vis range. Owing to wide bandgaps, the grown LHHCL and LHMDHCL crystals could be widely used in device applications that require high-temperature operations.

3.5 SHG study

Second harmonic generation (SHG) by the prepared samples was determined with the powder technique of Kurtz and Perry [41]. In this method, the LHHCL and LHMDHCL samples were crushed to fine microcrystallites and securely sandwiched between two clear glass surfaces. The optical source was a 1064 nm Nd: YAG laser with an 8 ns pulse width and 10 Hz pulse rate. The laser beam was directed onto a powder sample using a filter. The final output from

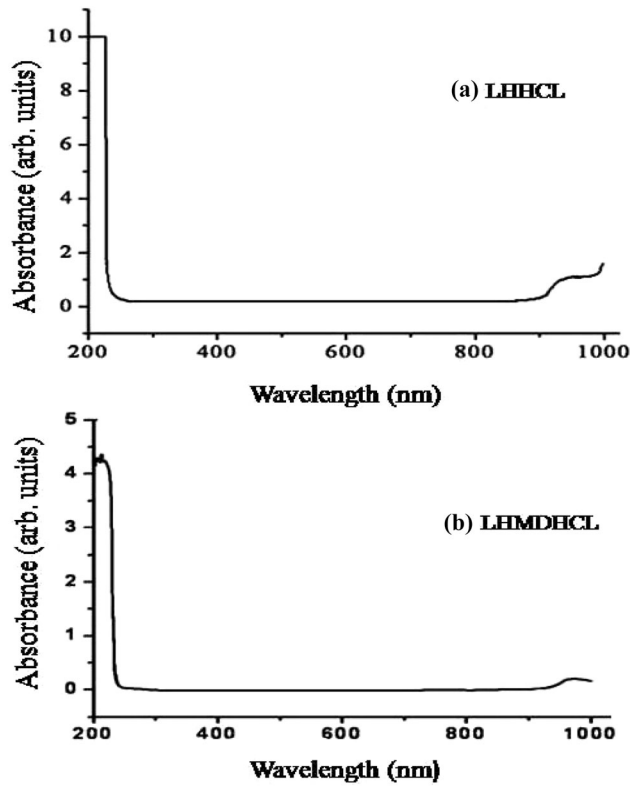


Fig. 4 UV-Vis absorbance spectra of a LHHCL and b LHMDHCL

the sample was presented on the oscilloscope. The samples generated the green signal, indicating that SHG pulses have been generated. The SHG performance was measured by using the fine powders of the KDP sample as reference material. According to the SHG test, the SHG performance of LHHCL is 3 times that of the KDP sample; whereas the SHG performance of LHMDHCL is 1.6 times that of the KDP sample.

3.6 Vickers hardness test

The hardness test is a popular method for determining the strength of the material in the microhardness range. Material strength, elasticity, and plasticity can all be replicated with a microhardness test. Static indentations on the grown crystals were performed at an ambient temperature with a Vickers-microhardness device and a diamond pyramidal indenter coupled to optical microscopy. To determine the hardness index (H_v), multiple indentations were formed on the crystalline samples with weights ranging from 10 to 50 g. Since the higher loads generated micro-cracks on the crystal surfaces, the

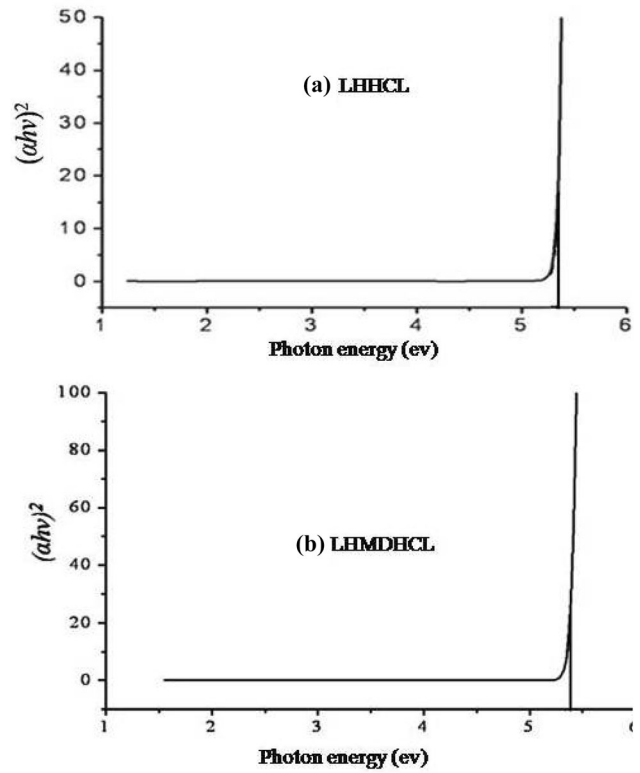


Fig. 5 Plots of $(\alpha hv)^2$ vs. hv for a LHHCL and b LHMDHCL

maximum load applied was limited to 50 g. For all the weight, the indentation time was kept to be 15 s. The micro-hardness index (H_v) was determined by using the relation

$$H_v = \frac{1.8544P}{d^2} \text{ Kg mm}^{-2}$$

Here, P is the load applied in kilogram, and d is the indentation's average diagonal width in mm. Figure 6 illustrates the change in hardness index (H_v) with load applied (P) for the LHHCL and LHMDHCL crystals. The microhardness index (H_v) for both LHHCL and LHMDHCL crystals diminishes as the load increases, which is consistent with the usual indentation size effect (ISE). The work hardening coefficient ' n ' has been calculated using the least square fit approach from the plot of $\log P$ vs. $\log d$ (Fig. 7). According to Onitsch's prediction, a material with a hardness coefficient $1.0 \leq n \leq 1.6$ is regarded as hard, whereas a material with hardness coefficient $n > 1.6$ is deemed soft [42]. By this assessment, the n value for LHHCL is calculated as 1.65; showing that LHHCL is a soft material, whereas the n value for LHMDHCL was found to be 1.46, suggesting that LHMDHCL is a hard material. Since

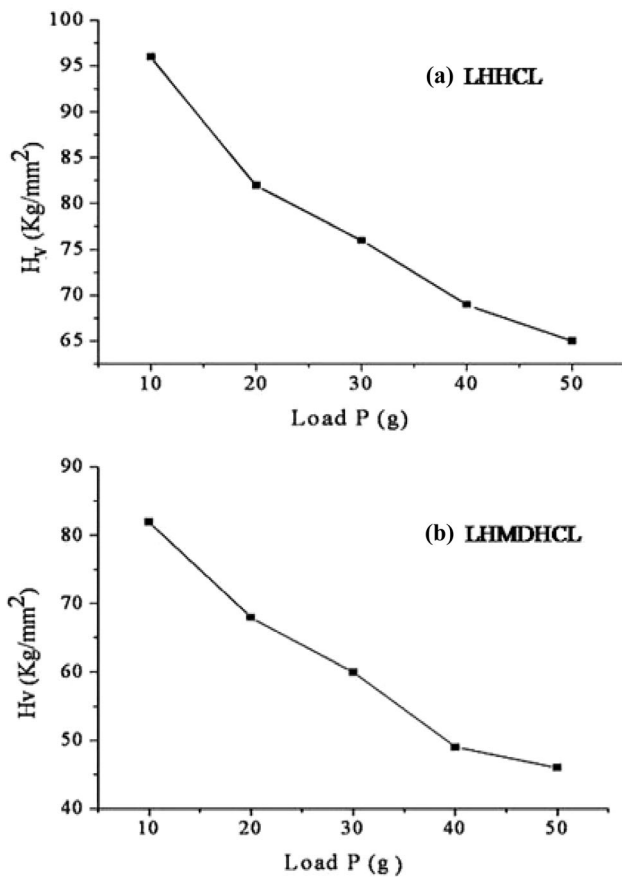


Fig. 6 Plots of hardness number (H_v) vs. applied load for **a** LHHCL and **b** LHMDHCL

the work hardening coefficient ' n ' for both crystals is less than 2, the material's hardness is found to decrease with applied load, validating Onitsch's prediction.

3.7 Dielectric study

The dielectric study is a method used for studying the electrical response of solid materials. It provides insight into the dynamics of the electric field within a material [43]. The dielectric constant and dielectric loss of the LHHCL and LHMDHCL crystals were measured using a HIOKI 35 LCR HITESTER as a function of temperature at frequencies ranging from 50 Hz to 5 MHz. Figure 8 depicts the decrease of dielectric constant with applied frequency for the LHHCL and LHMDHCL crystals. The dielectric constant has greater values in the low-frequency area and subsequently declines exponentially with the applied frequency, as seen by the curve. This could be explained in terms of the polarization phenomena;

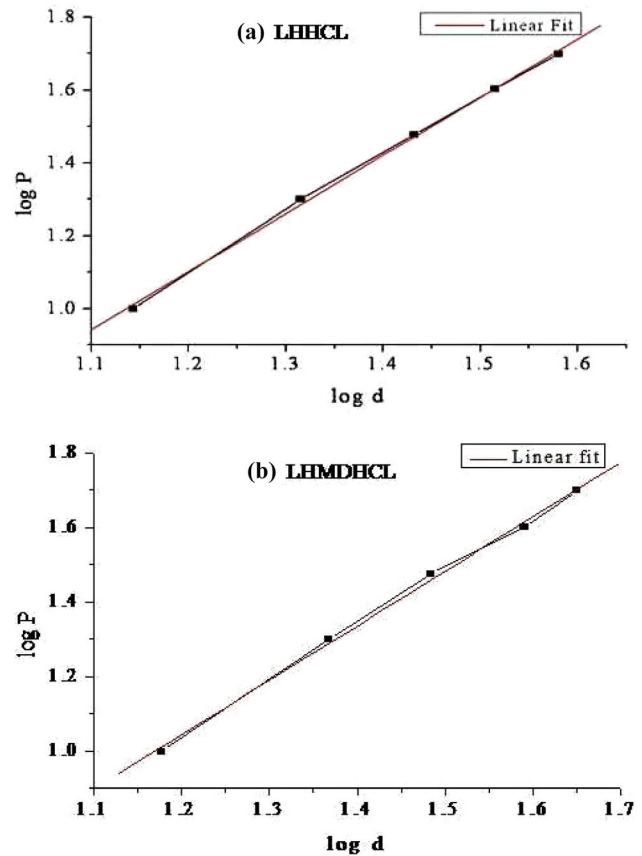


Fig. 7 Plots of $\log P$ vs. $\log d$ for **a** LHHCL and **b** LHMDHCL

the electronic exchange between an ion and lattice provides a local displacement of electrons in a given volume. In other words, polarization is caused by the electronic exchange between the two. As the frequency increases, the space charge decreases, affecting polarization and resulting in decreased dielectric constant values [44]. Furthermore, the dielectric constant of LHHCL increases with increasing temperature at low frequencies but remains constant at higher frequencies. However, the dielectric constant of LHMDHCL falls as temperature rises in all frequency range.

Figure 9 illustrates how the dielectric loss of LHHCL and LHMDHCL decreases exponentially with frequency and temperature. It has been observed that the dielectric loss shows a similar response as that of the dielectric constant for the grown crystals. The dielectric loss diminishes as the frequency rises, and it nearly disappears at higher frequencies. Furthermore, at lower frequencies, the dielectric loss increases slightly with increasing temperature, while at higher frequencies, it remains

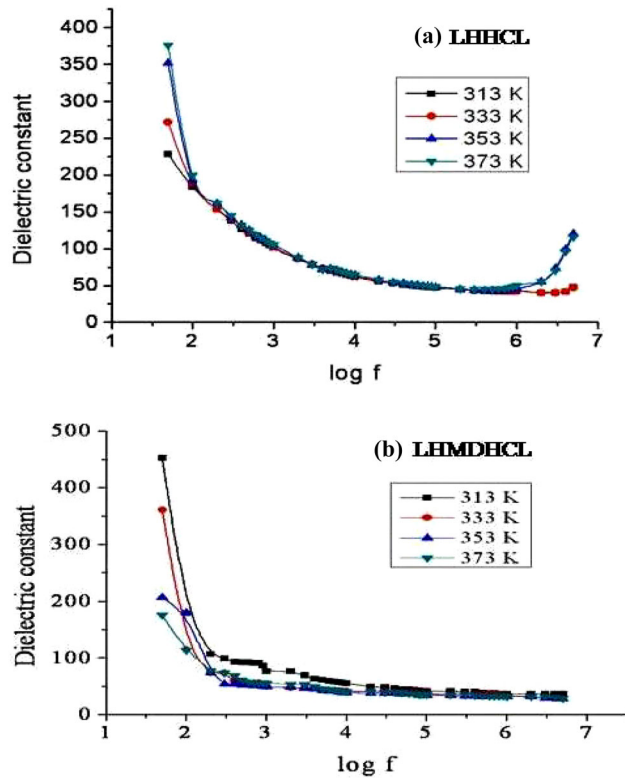


Fig. 8 Plots of dielectric constant vs. log frequency for **a** LHHCL and **b** LHMDHCL

constant regardless of temperature. As LHHCL and LHMDHCL crystals have such a lower dielectric constant and dielectric loss at high frequencies, they offer better optical transmittance and less imperfection, which is a desirable attribute for NLO applications.

4 Conclusion

The crystalline materials L-histidinium hydrochloride monohydrate (LHHCL) and L-histidinium methyl ester dihydrochloride (LHMDHCL) were effectively produced at ambient temperature using the slow evaporation technique. According to XRD analysis, LHHCL crystallized in orthorhombic space group $P2_12_12_1$, whereas the LHMDHCL crystallized in monoclinic space group $P2_1$. Identification of chemical groups and the formation of LHHCL and LHMDHCL crystals were confirmed using FT-Raman spectral analysis. The presence of oxygen, nitrogen, carbon, and chlorine in the appropriate ratio was proved by the EDAX spectra and hence confirming

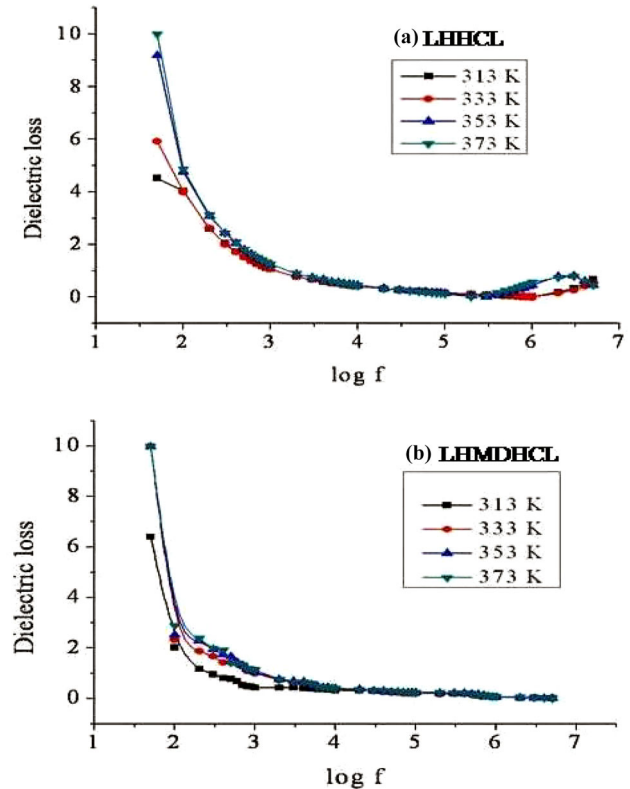


Fig. 9 Plots of dielectric loss vs. log frequency for **a** LHHCL and **b** LHMDHCL

the formation of the LHHCL and LHMDHCL crystals. The UV–Vis study substantiates the transparency of LHHCL and LHMDHCL in the wavelength ranges of 232–1000 and 230–1000 nm, respectively, validating the utility of the grown crystals for photonic applications. The bandgap energies were determined as 5.35 and 5.38 eV for LHHCL and LHMDHCL crystals, respectively. According to the SHG test, the SHG performance of LHHCL is 3 times that of the KDP sample; whereas the SHG performance of LHMDHCL is 1.6 times that of the KDP sample. Due to their low dielectric constant and dielectric loss on elevated frequency, LHHCL and LHMDHCL crystals have improved optical quality with less imperfection, which is a desirable attribute for NLO applications. Vickers microhardness study reveals that LHHCL belongs to the soft category while LHMDHCL belongs to the hard category of materials. The low dielectric constant and dielectric loss in the higher frequency range, as well as their comparatively high SHG performance, makes the LHHCL and LHMDHCL

crystals interesting materials for frequency doubling and laser applications.

Supplementary Information: The online version contains supplementary material available at <https://doi.org/10.1007/s10854-021-07495-w>.

References

- G.J. Shanmuga Sundar, S.M. Ravi Kumar, M. Packiya Raj, S. Selvakumar, *Mater. Res. Bull.* **112**, 22–27 (2019). <https://doi.org/10.1016/j.materresbull.2018.11.043>
- P. Krishnamoorthi, P. Sundaramoorthi, *J. Mater. Sci. Mater. Electron.* **32**, 21756–21769 (2021). <https://doi.org/10.1007/s10854-021-06696-7>
- E. Raju, P. Jayaprakash, G. Vinitha, N. Saradha Devi, S. Kumaresan, *J. Mater. Sci. Mater. Electron.* **32**, 21155–21163 (2021). <https://doi.org/10.1007/s10854-021-06614-x>
- M. Rajkumar, A. Chandramohan, *Mater. Lett.* **181**, 354–357 (2016). <https://doi.org/10.1016/j.matlet.2016.04.191>
- K. Xu, L. Cao, F. You, D. Zhong, T. Wang, Z. Yu, C. Hu, J. Tang, B. Teng, *J. Cryst. Grow.* **547**, 125757 (2020). <https://doi.org/10.1016/j.jcrysgro.2020.125757>
- Z.S. Feng, Z.H. Kang, F.G. Wu, J.Y. Gao, Y. Jiang, H.Z. Zhang, Y.M. Andreev, G.V. Lanski, V.V. Atuchin, T.A. Gavrilova, *Opt. Express.* **16**, 9978–9985 (2008). <https://doi.org/10.1364/OE.16.009978>
- V.V. Atuchin, A.K. Subanakov, A.S. Aleksandrovsky, B.G. Bazarov, J.G. Bazarov, T.A. Gavrilova, A.K. Krylov, M.S. Molokeev, A.S. Oreshonkov, S.Y. Stefanovich, *Mater. Des.* **140**, 488–494 (2018). <https://doi.org/10.1016/j.matdes.2017.12.004>
- E.V. Alekseev, O. Felbinger, S. Wu, T. Malcherek, W. Depmeier, G. Modolo, T.M. Gesing, S.V. Krivovichev, E.V. Suleimanov, T.A. Gavrilova, L.D. Pokrovsky, A.M. Pugachev, N.V. Surovtsev, V.V. Atuchin, *J. Solid State Chem.* **204**, 59–63 (2013). <https://doi.org/10.1016/j.jssc.2013.04.038>
- Ish. Steinberg, A.V. Kirpichnikov, V.V. Atuchin, *Opt. Mater.* **78**, 253–258 (2018). <https://doi.org/10.1016/j.optmat.2017.11.025>
- P. Karuppasamy, D. Joseph Daniel, H.J. Kim, M. Senthil Pandian, P. Ramasamy, *J. Cryst. Grow.* **535**, 125528 (2020). <https://doi.org/10.1016/j.jcrysgro.2020.125528>
- S. Devi, D. Jananakumar, *Appl. Phys. A* **126**, 394 (2020). <https://doi.org/10.1007/s00339-020-03571-w>
- R. Divya, V.T. Vineeth, B.R. Bijini, C.M.K. Nair, K. RajendraBabu, *J. Mole. Struct.* **1200**, 127031 (2020). <https://doi.org/10.1016/j.molstruc.2019.127031>
- P. Karuppasamy, M. Senthil Pandian, P. Ramasamy, S.K. Das, *Optik* **156**, 707–719 (2018). <https://doi.org/10.1016/j.ijleo.2017.12.012>
- S. Shanmugan, N. Saravanan, V. Chithambaram, B. Deepanraj, G. Palani, *Bull. Mater. Sci.* **43**, 202 (2020). <https://doi.org/10.1007/s12034-020-02176-6>
- J. Palaninathan, V. Rathinam, A.B. Ali Baig, V. Rathinam, V. Ramya, *J. Mater. Sci. Mater. Electron.* **36**, 6820–6829 (2021). <https://doi.org/10.1007/s10854-021-05387-7>
- M.R. Hareeshkumar, G.J. Shankaramurthy, A. Alhadhrami, M.R. Jagadeesh, B.M. Prasanna, *Iran. J. Sci. Technol. Trans. Sci.* **45**, 1843–1850 (2021). <https://doi.org/10.1007/s40995-021-01160-x>
- H.O. Marcy, M.J. Rosker, L.F. Warren, P.H. Cunningham, C.A. Thomas, *Opt. Lett.* **20**, 252–254 (1995). <https://doi.org/10.1364/OL.20.000252>
- J. Madhavan, S. Aruna, A. Anuradha, D. Premanand, I. Vetha Potheher, *Opt. Mater.* **29**, 1211–1216 (2007). <https://doi.org/10.1016/j.optmat.2006.04.013>
- J. Madhavan, S. Aruna, K. Praba, J.P. Julius, J. Jinson, P. Joseph, S. Selvakumar, P. Sagayaraj, *J. Cryst. Grow.* **293**, 409–414 (2006). <https://doi.org/10.1016/j.jcrysgro.2006.05.050>
- S. Aruna, M. Vimalan, P.C. Thomas, K. Thamizharasan, K. Ambugam, J. Madhavan, P. Sagayaraj, *Cryst. Res. Technol.* **42**, 180–185 (2007). <https://doi.org/10.1002/crat.200610793>
- H.A. Petrosyan, H.A. Karapetyan, A.M. Petrosyan, *J. Mol. Struct.* **794**, 160–167 (2006). <https://doi.org/10.1016/j.molstruc.2006.02.004>
- H.A. Petrosyan, H.A. Karapetyan, A.K. Atanesyan, A.M. Petrosyan, *J. Mol. Struct.* **963**, 168–174 (2010). <https://doi.org/10.1016/j.molstruc.2009.10.030>
- J. Ramajothi, S. Danuskodi, *Spect. Chim. Acta A.* **68**, 1213–1219 (2007). <https://doi.org/10.1016/j.saa.2007.01.030>
- M. Fleck, V.V. Ghazaryan, L.S. Bezhanova, A.K. Atanesyan, A.M. Petrosyan, *J. Mol. Struct.* **1035**, 407–415 (2013). <https://doi.org/10.1016/j.molstruc.2012.11.067>
- J. Ramajothi, S. Dhanuskodi, *Cryst. Res. Technol.* **38**, 592–597 (2004). <https://doi.org/10.1002/crat.200310229>
- G.H. Sun, X.T. Sun, Z.H. Sun, X.Q. Wang, X.J. Liu, G.H. Zhang, D. Xu, *J. Cryst. Grow.* **311**, 3904–3910 (2009). <https://doi.org/10.1016/j.jcrysgro.2009.06.022>
- H.M. Albert, A. Joseph Arul Pragasam, G. Bhagavanarayanan, C. Alosious Gonsago, *J. Therm. Anal. Calorim.* **118**, 333–338 (2014). <https://doi.org/10.1007/s10973-014-4007-9>
- J. Chandrasekaran, P. Ilayabarathi, P. Maadeswaran, P. Mohamed Kutty, S. Pari, *Opt. Commun.* **285**, 2096–2100 (2012). <https://doi.org/10.1016/j.optcom.2011.12.063>

29. P. Catherine, P. Praveen Kumar, B. Gunasekaran, *Opt. Quant. Elect.* **53**, 191 (2021). <https://doi.org/10.1007/S11082-021-02830-1>
30. J. Donohue, A. Caron, *Acta Crystallogra.* **17**, 1178 (1964). <https://doi.org/10.1107/S0365110X64003048>
31. V.H. Vilchiz, R.E. Norman, S.C. Chang, *Acta Crystallogr. C.* **51**, 696–698 (1996). <https://doi.org/10.1107/s0108270195013308>
32. S. Balaprabhakaran, J. Chandrasekaran, B. Babu, R. Thirumurugan, K. Anitha, *Spect. Chim. Acta A* **136**, 700–706 (2015). <https://doi.org/10.1016/j.saa.2014.09.084>
33. N.R. Rajagopalan, P. Krishnamoorthy, *Optik* **127**, 3582–3589 (2016). <https://doi.org/10.1016/j.ijleo.2015.12.153>
34. G. Herzberg, B.L. Crawford Jr., *J. Phys. Chem.* **50**, 288 (1946). <https://doi.org/10.1021/j150447a021>
35. J.R. Ferraro, K. Nakamoto, C.W. Brown, *Introductory Raman Spectroscopy*, 2nd edn. (Academic Press, Amsterdam, 2003)
36. C.K. Bhat, C.L. Bhat, P.K. Madan Lal, P.K. Patra, P.N. Kotru, *X-ray Spectrom.* **23**, 247–250 (1994). <https://doi.org/10.1002/xrs.1300230603>
37. E. Cook, R. Fong, J. Horrocks, D. Wilkinson, R. Speller, *Appl. Rad. Isoto.* **65**, 959–967 (2007). <https://doi.org/10.1016/j.apradiso.2007.02.010>
38. V.H. Mudavakkat, V.V. Atuchin, V.N. Kruchinin, A. Kayani, C.V. Ramana, *Opt. Mater.* **34**, 893–900 (2012). <https://doi.org/10.1016/j.optmat.2011.11.027>
39. V.V. Atuchin, A.K. Subanakov, A.S. Aleksandrovsky, B.G. Bazarov, J.G. Bazarova, S.G. Dorzhieva, T.A. Gavrilova, A.S. Krylov, M.S. Molokeev, A.S. Oreshonkov, A.M. Pugachev, Y.L. Tushinova, A.P. Yelisseyev, *Adv. Powd. Technol.* **28**, 1309–1315 (2017). <https://doi.org/10.1016/j.appt.2017.02.019>
40. J. Tauc, R. Grigorovici, A. Vancu, *Phys. Stat. Soli. B.* **15**, 627–637 (1966). <https://doi.org/10.1002/pssb.19660150224>
41. S.K. Kurtz, T.T. Perry, *J. Appl. Phys.* **39**, 3798–3813 (1968). <https://doi.org/10.1063/1.1656857>
42. T. Sivanandan, S. Kalainathan, *Mater. Lett.* **162**, 211–213 (2016). <https://doi.org/10.1016/j.matlet.2015.10.009>
43. K. Senthil, K. Elangovan, A. Senthil, G. Vinitha, *Spect. Chim. Acta A.* **247**, 119063 (2021). <https://doi.org/10.1016/j.saa.2020.119063>
44. P. Sagunthala, V. Veeravazhuthi, P. Hemalatha, P. Yasotha, *Ferroelect.* **504**, 96–103 (2016). <https://doi.org/10.1080/00150193.2016.1239487>

Publisher's Note Springer Nature remains neutral with regard to jurisdictional claims in published maps and institutional affiliations.